Applied Catalysis B: Environmental 254 (2019) 37–46

Contents lists available at ScienceDirect

Applied Catalysis B: Environmental

journal homepage: www.elsevier.com/locate/apcatb

Pore-functionalized ceramic membrane with isotropically impregnated cobalt oxide for sulfamethoxazole degradation and membrane fouling elimination: Synergistic effect between catalytic oxidation and membrane separation

Yueping Bao[a,b], Wen Jie Lee[a,b], Teik-Thye Lim[b,c,*], Rong Wang[b,c], Xiao Hu[b,d,**]

[a] Interdisciplinary Graduate School, Nanyang Technological University, 637141, Singapore
[b] Nanyang Environment and Water Research Institute, Nanyang Technological University, 637141, Singapore
[c] School of Civil and Environmental and Engineering, Nanyang Technological University, 639798, Singapore
[d] School of Materials Science and Engineering, Nanyang Technological University, 639798, Singapore

ARTICLE INFO

Keywords:
Self-sacrificed template
Fouling
Regeneration
Sulfate radical
Synergistic coupling

ABSTRACT

In this study, a pore-functionalized ceramic membrane with isotropically impregnated cobalt oxide (CoCM) was prepared *via* an *in-situ* self-sacrificed template method and applied for sulfamethoxazole (SMX) degradation by peroxymonosulfate (PMS) activation under a dead-end membrane filtration mode. The physical and chemical properties of the membranes were characterized *via* FESEM, AFM, XRD and XPS. Results indicated that Co_3O_4 had been impregnated into the macropores uniformly throughout the whole ceramic membrane without pore blocking. The formation of Co—O—Al bonding inhibited the leaching of cobalt during the filtration while the hydroxyl group Co − OH played a crucial role during the radical generation. The contact angle of CoCM decreased, resulting in a higher pure water permeability as compared to the original ceramic membrane. The catalytic degradation of SMX showed that its removal efficiency could be influenced by both contact time and PMS dosage. CoCM exhibited superior antifouling property during the humic acid (HA) removal study. The stability and regeneration of CoCM were investigated. Furthermore, the radical quenching experiment was conducted and the concentration of sulfate radical was quantitatively estimated. Finally, the PMS activation as well as organics removal mechanism in CoCM *via* the synergistic coupling of catalytic Co_3O_4 and membrane separation were proposed.

1. Introduction

The intensive use of antibiotics for human, veterinary and agricultural purposes results in their continuous release into the environment [1,2]. The major concern in relation to that is the development of antibiotic resistance genes and bacteria, which would reduce the therapeutic potential against human and animal pathogens [3]. Non-conventional water treatment technologies, including phase-changing technology, biological treatment and advanced oxidation processes (AOPs) have been investigated for the removal of antibiotics. Generally, it is well-accepted that the removal efficiency of antibiotics using AOPs is much higher compared with other technologies [4]. Sulfate radical based advanced oxidation processes (SR-AOPs) have been recognized as an effective alternative method to the destruction of recalcitrant organics in wastewater, in which highly-reactive sulfate radical was generated and utilized to oxidize organic contaminants to innocuous CO_2 and H_2O [5]. Lots of works have been conducted to develop new methods for sulfate radical generation [6,7]. Among the most commonly accepted method includes peroxymonosulfate (PMS) activation *via* metal oxides, in which cobalt based catalysts have been identified as the most efficient PMS activator [8]. The heterogeneous Co/PMS system is favorable in practical applications because it can minimize the adverse effect of cobalt ions on human health [9]. So far, various supporting materials including resin, zeolite, Al_2O_3 and mesoporous

* Corresponding author at: School of Civil and Environmental and Engineering, Nanyang Technological University, Block N1-01b-47, 50 Nanyang Avenue, 639798, Singapore.
** Corresponding author at: School of Materials Science and Engineering, Nanyang Technological University, Block N4.1-01-14, 50 Nanyang Avenue, 639798, Singapore.
E-mail addresses: cttlim@ntu.edu.sg (T.-T. Lim), ASXHU@ntu.edu.sg (X. Hu).

https://doi.org/10.1016/j.apcatb.2019.04.081
Received 17 December 2018; Received in revised form 19 March 2019; Accepted 23 April 2019
Available online 27 April 2019
0926-3373/

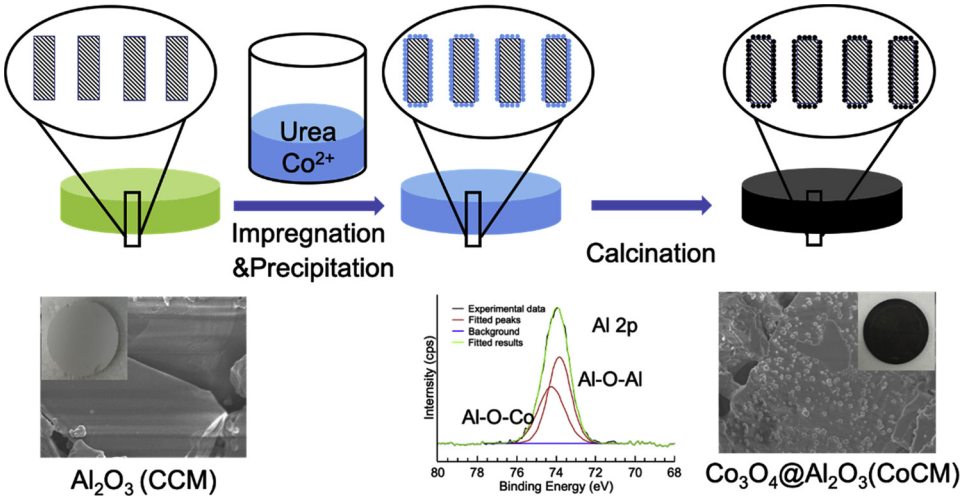

Fig. 1. The preparation of Co_3O_4 impregnated ceramic membrane (CoCM).

carbon have been designed and used to immobilized cobalt-based catalysts for PMS activation [10–13]. However, most of them are suspended in water during use and therefore need a further separation process.

On the other hand, microfiltration (MF) has been proved to be a promising technology for water purification in recent decades because of the high yield of production and low energy consumption [14]. However, the membrane fouling caused by the exposure of membranes to a broad range of foulants results in a substantial decrease in their water permeability, which leads to a high permeate loss and energy consumption [15]. Meanwhile, the separation principle for MF is based on size exclusion, which means it cannot remove many kinds of organic micro-pollutants during the physical separation process, resulting in the effluent discharge with potential hazard [16]. To overcome these drawbacks, one possible solution is the integration of MF with AOPs (*e.g.*, photocatalysis, Fenton and ozonation) in the treatment system [17–21]. In the integration process, intrinsic catalytic degradation of organic contaminants prevents them from permeating through the membrane without treatment. Simultaneously, the inherent membrane fouling can be mitigated *via* the incorporation of reactive nanocatalysts that can generate reactive oxygen species (ROS) to degrade the foulants on the membrane surface or inside the pores.

Herein, an integrated system with membrane filtration and SR-AOP could be employed to enhance the membrane performance as well as to avoid the catalyst recycling. In the previous study, a cobalt oxide functionalized ceramic membrane was developed for organics degradation in a membrane filtration system [22]. The surface modification changed the morphology as well as chemical properties of the ceramic membrane, and the catalytic performance test confirmed the radical generation process. However, the active sites on the membrane surface were limited by surface modification and the intermediate products could still pass through the membrane without further degradation. Meanwhile, there is still limited study on the mechanism of catalytic membrane for PMS activation, especially the synergistic effect between catalyst and membrane.

Therefore, in this work, we developed a novel pore-functionalized ceramic membrane with isotropically impregnated Co_3O_4 (CoCM) *via* an *in-situ* self-scarified template method. It is the first report on the pore-functionalized ceramic membrane with Co_3O_4 for PMS activation. Meanwhile, the performance of CoCM was investigated *via* sulfamethoxazole (SMX) degradation and humic acid (HA) removal in the membrane filtration system. Finally, the PMS activation as well as organics removal mechanism *via* synergistic effect between Co_3O_4 and ceramic membrane in the CoCM were proposed and the sulfate radical generated in the process was quantified.

2. Experimental

2.1. Chemicals and materials

Sulfamethoxazole (SMX), cobalt(II) nitrate hexahydrate ($Co(NO_3)_2{\cdot}6H_2O$), manganese (II) nitrate tetrahydrate ($Mn(NO_3)_2{\cdot}4H_2O$), nickel (II) nitrate hexahydrate ($Ni(NO_3)_2{\cdot}6H_2O$), humic acid (HA), glacial acetic acid ($C_2H_4O_2$), methanol (MeOH, CH_4O), *tert*-butanol (TBA, $C_4H_{10}O$), ceric sulfate tetrahydrate ($CeH_8O_{12}S_2$) and cerium(III) sulfate octahydrate ($Ce_2(SO_4)_3{\cdot}8H_2O$) were purchased from Sigma-Aldrich. Urea (CH_4N_2O) was supplied by VWR. Potassium peroxymonosulfate ($2KHSO_5{\cdot}KHSO_4{\cdot}K_2SO_4$ available as Oxone, PMS) was supplied by Alfa Aesar. All solutions were prepared in deionized (DI) water (18.2 MΩ cm at 25 °C) from a Milli-Q purification system while all chemicals were of reagent grade or higher and were used without further purification.

The commercial porous Al_2O_3 ceramic membrane was purchased from Nanjing Shuyihui Scientific Instruments CO., LTD (Nanjing, China). The as received membranes were disc shaped with a diameter of 22 mm and a thickness of 2 mm, hereafter referred as controlled ceramic membrane (CCM). Prior to use, the CCMs were immersed into NaOH (0.5 M) and DI water for 30 min each followed by washing and drying at 120 °C overnight.

2.2. Preparation of Co_3O_4 impregnated ceramic membrane (CoCM)

A pore-functionalized ceramic membrane with isotropically impregnated Co_3O_4 was developed *via* an *in-situ* self-scarified template method (Fig. 1) in which Urea was used as the self-scarified template. Urea has been served well as a precipitant because it can decompose very slowly at 90 °C in aqueous media according to the following reaction Eq. (1) [23]. Consequently, hydroxyl groups are formed slowly and uniformly throughout the membrane pores, followed by the metal hydroxides precipitation taking place homogeneously.

$$CO(NH_2)_2 + 3H_2O \rightarrow 2OH^- + 2NH_4^+ + CO_2\ (90\ ^\circ C) \quad (1)$$

As demonstrated in Fig. 1, the ceramic membrane was first immersed into the precursor solution (containing a certain amount of cobalt nitrate and urea) for 30 min. After the excess solution was drained off, the wet membrane was put into an oven at 90 °C for 12 h, resulting in precipitation of metal hydroxide *via* the slow hydrolysis of urea in the membrane pores. After the reaction, the membrane was washed with DI water followed by drying at 90 °C overnight. To decompose the precipitated metal hydroxide to metal oxides, the membrane was heated at 5 °C min^{-1} till 450 °C and calcined for 3 h in an air

atmosphere. The resulted membrane was named as CoCM. Since this work focused on the new method to develop a catalytic ceramic membrane and its application in a hybrid system, the concentration of precursors is not optimized in the current work. A fixed concentration of 10 mM $Co(NO_3)_2{\cdot}6H_2O$ and 15 mM Urea in DI water was used for all the experiments.

2.3. Characterization methods

The crystalline composition of CCM and CoCM as well as metal oxides particles was characterized by X-ray diffraction (XRD, Bruker D8 Advance) from 15° to 75° with a step size of 0.02° combined with a rotation rate of 15 rpm. The operating parameters were set at 40 kV and 40 mA using Cu-K_α (λ = 1.54 Å) radiation. The surface morphologies of the as-prepared membranes were obtained by field emission scanning electron microscope (FESEM, JSM-7600 F, JEOL, Japan). Atomic force microscopy (AFM, Park XE-100) was employed to measure the membrane surface properties and roughness. Surface hydrophilicity of the membranes was analyzed by measuring the water contact angle using the sessile drop method with a contact angle goniometer (DataPhysics OCA 15EC), with a digital camera recording the shape change of each liquid droplet tested. Furthermore, X-ray photoelectron spectroscopy (XPS) measurement was conducted on a Kratos Axis Supra spectrophotometer (Shimadzu) equipped with a dual anode monochromatic Kα excitation source ($h\nu$ = 1486.7 eV) to analyze the chemical states of elements. All binding energies for elements of interest were corrected against an adventitious carbon C 1s core level at 284.6 eV and all XPS peaks were fitted using Shirley background together with Gaussian-Lorentzian function.

The overall porosity ε (%) of membrane, which is defined as the volume of the pores divided by the total volume of the membrane was calculated by a dry-wet weight method through the following equation Eq. (2).

$$\varepsilon = \frac{\frac{W_{wet} - W_{dry}}{\rho_{H_2O}}}{\frac{W_{wet} - W_{dry}}{\rho_{H_2O}} + \frac{W_{dry}}{\rho_{CM}}} \quad (2)$$

where W_{wet} and W_{dry} represent the weights of wet and dry membranes, ρ_{H2O} and ρ_{CM} are the density of DI water and Al_2O_3 membrane.

2.4. Performance evaluation

The water permeability, catalytic performance and antifouling properties of the membranes were evaluated through a home-made dead-end filtration system. The schematic diagram of the experimental setup is shown in Fig S1 which contains two metering pumps and one balance for permeate recording. In the filtration experiment, the membrane was fitted into a circular membrane cell, the feed (SMX/HA) and oxidant (PMS) solutions were pumped separately and mixed just before entering the membrane cell. The effects of contact time and PMS dosage were investigated.

The pure water permeate flux was measured by varying the transmembrane pressure (TMP) in the range of 0.1 − 0.5 bar. The mass of permeate was measured and converted to permeate flux according to the Eq. (3) and the intrinsic membrane resistance R_m (m^{-1}) is defined by Eq. (4).

$$J = V / A\ t \quad (3)$$

$$R_m = (\Delta P)\ A\ t / \mu\ V \quad (4)$$

where J represents permeate flux (LMH), V is volume of permeate (L), A is effective membrane surface area (m^2), t represents the filtration time (h), ΔP means the transmembrane pressure (TMP, Pa) and μ is the kinematic viscosity of water (1×10^{-3} Pa s).

The catalytic performance was evaluated by degradation of SMX ($C_{10}H_{11}N_3O_3S$, MW = 254 g mol^{-1}), which is found ubiquitous in the aquatic system and responsible for the development of antibiotic resistance [3]. The rejection and antifouling tests were performed with an aqueous solution of humic acid (HA). All the filtration processes were carried out at room temperature under a constant flow of 236 LMH and the trans-membrane pressure (TMP) was recorded. In a typical filtration experiment, the feed (SMX/HA) and oxidant (PMS) were mixed before the membrane cell and the concentration of SMX/HA in the permeate side was analyzed. The effects of contact time as well as PMS dosage were investigated by changing the flow rate and PMS concentration.

2.5. Determination of chemicals and degradation products

The concentration of SMX was determined using a liquid chromatography system (Shimadzu, LC-2030C-3D) equipped with an Inertsil ODS-3 column (4.6 × 150 mm;5 μm). The mobile phase was an isocratic mixture with 60% methanol and 40% acetic water (0.1% v/v). The flow rate was set at 0.8 m L min^{-1}. The UV detector was operated at a wavelength of 264 nm and the injection volume is 10 μ L. The intermediates were further analyzed using an Agilent 1290 Infinity HPLC coupled to an Agilent 6460 Triple quadruple mass spectrometry, which was equipped with an Electrospray ionization (ESI) source using Agilent Jet Stream Technology (Agilent, USA). The mobile phases consisted of water with 0.1% formic acid and acetonitrile with 0.1% formic acid. Separations were performed using a 75 mm × 2 mm Luna 3μ C18 column with a flow rate of 0.2 m L min^{-1}. A gradient elution method with two mobile phases was employed as follows: 90% A for 0–0.5 min; 90% A decreased to 10% A lineally for 0.5–5.5 min and kept for 5.5–8.0 min; 10% A increased to 90% A lineally for 8.0–9.5 min and kept for 9.5–10.0 min.

The total organic carbon (TOC) was analyzed before and immediately after the filtration using a TOC analyzer (Shimadzu TOC-L analyzer). The concentrations of dissolved metals were measured using the inductively coupled plasma optical emission spectrometry (ICP-OES, Perkin Elmer, Optima 8000). PMS and HA were quantified by UV-1800 spectrophotometer (Shimadzu, Japan) at UV_{352} Eq. (5) and UV_{300} [22].

$$I^- + HSO_5^- + 2H^+ \rightarrow HSO_4^- + I_3^- + H_2O \quad (5)$$

A spectrophotometric determination method was used to quantify the sulfate radical concentration in aqueous solutions. As described in the literatures, cerium (III) could be oxidized by sulfate radical to form Ce(IV) Eq. (6) in which other radicals ($^1O_2$, •OH and $O_2^{-\bullet}$) have shown a negligible effect [24]. The generated Ce(IV) was then quantitated by UV-1800 spectrophotometer (Shimadzu, Japan) at UV_{320}. The calibration curves for PMS, HA and Ce(IV) are shown in Fig S2.

$$SO_4^{\bullet -} + Ce(III) \rightarrow SO_4^{2-} + Ce(IV),\ k = 1.43 \pm 0.3 \times 10^8\ M^{-1}s^{-1} \quad (6)$$

3. Results and discussions

3.1. Chemical and physical characterizations

FESEM characterizations of both surface and cross section (internal pores) of CCM and CoCM are displayed in Fig. 2. The CCM showed a smooth surface as well as internal pores, while it changed significantly after the Co_3O_4 impregnation. As shown in Fig. 2d and e, after the impregnation, the Co_3O_4 could be distributed evenly on the membrane surface as well as internal pores. No obvious catalytic separation layer was observed in the images, meaning there was no Co_3O_4 compact skin layer on the membrane surface. The AFM images show that there was no significant difference after the impregnation of Co_3O_4 (Fig. 2c and f).

XRD was used to characterize the structural and crystallographic properties of the as-prepared Co_3O_4 (Fig. 2g). The diffraction pattern

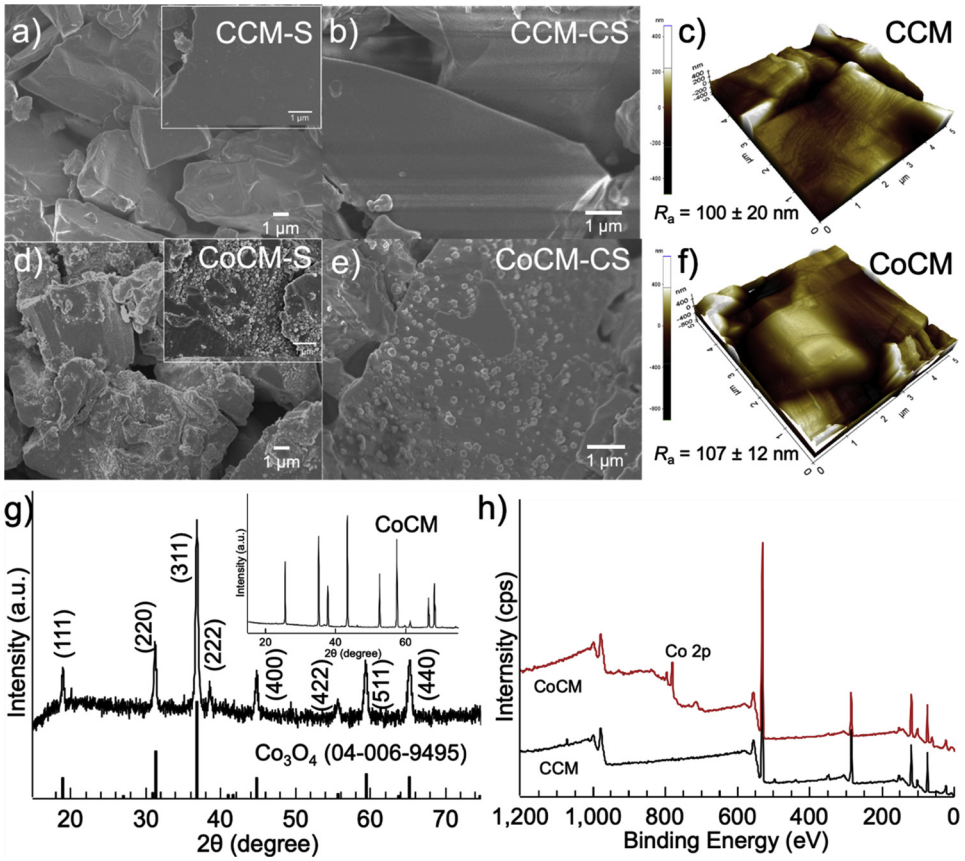

Fig. 2. Chemical and physical characterizations (a-FESEM of CCM surface; b-FESEM of CCM cross-section; c-AFM of CCM surface; d-FESEM of CoCM surface; e-FESEM of CoCM cross-section; f-AFM of CoCM surface; g-XRD of both Co_3O_4 particle and CoCM (Inset); h-XPS wide scan for both CCM and CoCM).

for the Co_3O_4 has eight broad peaks at 18.9°, 31.5°, 37.0°, 38.5°, 44.8°, 55.6°, 59.8° and 65.7°, corresponding to (111), (220), (311), (222), (400), (422), (511) and (440) of cubic Co_3O_4 (Entry No. 04-006-9495), respectively. The CoCM was also characterized (Inset of Fig. 2g). Results show that only Al_2O_3 phase was identified, which should be caused by the less impregnated amount of Co_3O_4 as well as extremely high signal of Al_2O_3.

To further analyze the bonding mechanism of CoCM, XPS analysis was carried out by investigating the various elemental chemical oxidation states in both CCM and CoCM. As shown in Fig. 2h, Co 2p was observed in the XPS survey spectrum in CoCM, demonstrating the successful impregnation of Co_3O_4. The spectrum of Al 2p shown in Fig. 3a could be readily assigned to Al-O, indicating the CCM surface is mainly covered by the Al_2O_3. However, the Al 2p spectrum (Fig. 3c) in CoCM could be fitted into two peaks which are corresponded to Al-O-Al and Co-O-Al, respectively. The existence of Co—O—Al bond could avoid Co_3O_4 aggregation as well as decrease the leaching of Co during the filtration test, improving the stability of CoCM. For both CCM and CoCM, two O 1s sub-peaks can be resolved with their binging energies at around 532 and 531 eV, which could be assigned to hydroxyl species (O_B) and lattice oxygen species (O_A), respectively [25]. On the surface of CoCM, the ratio of O_A/O_B is significantly increased to 3.46 (Fig. 3d) from 1.06 for CCM (Fig. 3b) due to the contribution of oxide from the Co_3O_4. Meanwhile, the presence of the surface hydroxyl groups can lead to the formation of Co − OH complex, which is crucial for the sulfate radical generation [26]. High resolution XPS of Co 2p further revealed the successful synthesis of Co_3O_4, in which the peaks appear at around 781 and 796 eV are ascribed to $Co2p_{3/2}$ and $Co2p_{1/2}$ (Fig. 3e).

3.2. Characterization of membrane properties

A summary of the membrane properties of CCM and CoCM is shown in Table 1. The porosity of CoCM was calculated as 41.9 ± 0.4% Eq. (2), which was similar to that of the original membrane (CCM). The comparable porosity revealed that Co_3O_4 was formed conformally on the surface of Al_2O_3 grains, without blocking the pores of the membranes, which could also be evidenced by FESEM images (Fig. 2). After impregnation with Co_3O_4, the weight of ceramic membrane increased slightly from 1518 ± 22 mg (CCM) to 1535 ± 11 mg (CoCM). The calculated Co_3O_4 loading amount was estimated as 1.1 wt% and it is believed that the loading amount could be controlled by changing the concentrations of precursors.

The roughness and hydrophilicity of membrane surface are significant factors influencing the permeability and antifouling properties of membranes. The surface roughness for CCM and CoCM was estimated *via* AFM (Fig. 2c and f) as 100 ± 20 nm and 107 ± 12 nm. The hydrophilicity of membrane surface was estimated through water contact angle between the air-water interface and the membrane surface, which reflects the wettability of the membrane surface [27]. As compared with the CCM which had a contact angle of 73.5 ± 3.4°, the contact angle of CoCM decreased to 52.4 ± 5.3°.

The pure water permeability of membranes was investigated in the home-made dead-end filtration system (Fig S1). Results showed that with imprganation of Co_3O_4, the pure water permeability increased from 3960 ± 330 to 7902 ± 527 LMHB while the intrinsic membrane resistance decreased from 9.16 to 4.58 × 10^{10} m^{-1}, corresponding to the changes of membrane surface hydrophilicity (Table 1). These observations confirmed that hydrophilicity and wettability of the ceramic membranes can be improved by the impregnation of Co_3O_4 *via* the as described *in-situ* self-sacrified template method.

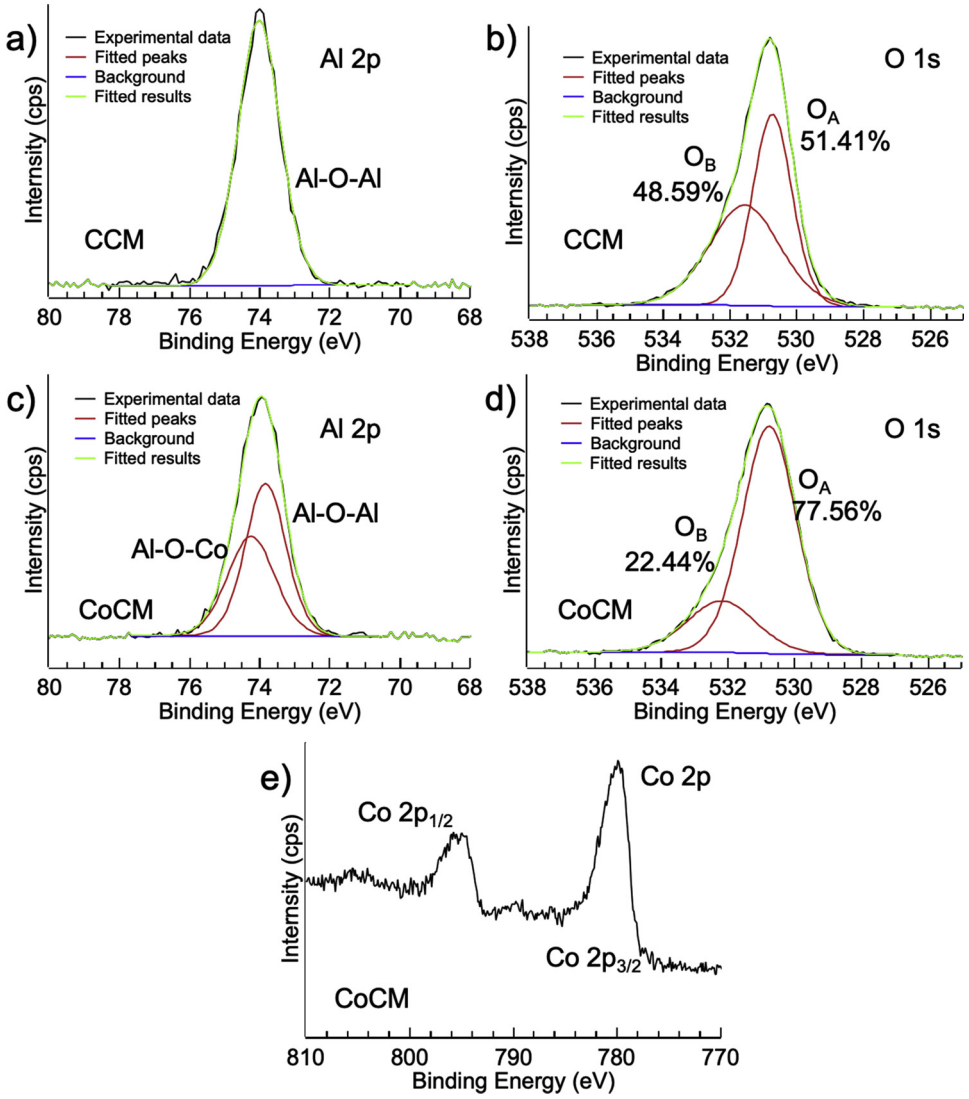

Fig. 3. High resolution of Al 2p, O 1 s and Co 2p in CCM and CoCM.

Table 1
Summary on the membrane properties of CCM and CoCM.

Membranes	Weight (mg)	Porosity (%)	Surface Roughness (nm)	Contact Angle (°)	Permeability (LMHB)	Intrinsic membrane resistance (m^{-1})
CCM	1518 ± 22	41.8 ± 0.5	100 ± 20	73.5 ± 3.4	3960 ± 330	9.16×10^{10}
CoCM	1535 ± 11	41.9 ± 0.4	107 ± 12	52.4 ± 5.3	7902 ± 527	4.58×10^{10}

3.3. Membrane performance in SMX removal

Fig. 4 illustrates the removal of SMX in membrane filtration system. When SMX was fed into the system, the removal efficiency was around 25% for CCM while it increased to 59% when CoCM was employed (Fig. 4a). Because of the low molecular size of SMX, the microfiltration membrane cannot reject it based on the molecular sieving mechanism. Meanwhile, there was no significant change in TMP throughout the filtration experiment (100 min), further indicating the negligible membrane fouling arising from the SMX accumulation on the membrane surface (Fig. 4b). Therefore, the removal of SMX should be attributed to its catalytic degradation. The metal leaching test showed Co_3O_4 was quite stable in CoCM with a low detected concentration of Co (0.045 ± 0.004 mg L^{-1}) in the permeate (Fig. 4b).

The effects of contact time and PMS dosage on SMX removal over CoCM in the membrane filtration system were further investigated. The results showed that with increase of flux from 236 to 708 LMH, the retention time was decreased from 16.8 to 5.6 s, resulting in the decrease of SMX removal from 59% to 20% (Fig. 4c). Meanwhile, being the source of free radicals, increasing PMS dosage caused more PMS to occupy the active sites, improving the probability of PMS and CoCM interaction, resulting in a higher SMX removal efficiency (Fig. 4d).

Even at 60% SMX removal efficiency for CoCM when the flux was set at 236 LMH and the PMS dosage was 0.8 mM, the TOC removal was only 15.3% (Fig S3). The results showed that the SMX was mostly degraded into smaller molecules but not mineralized to CO_2 and H_2O. The intermediate products were analyzed by LC-MS-MS (Fig S4) and the proposed degradation pathway involved i) the cleavage of sulfonamide bond, ii) OH addition and iii) electron transfer reaction (Fig. 4e) [28]. The cleavage of sulfonamide bond (i) was most likely caused by the PMS direct oxidation *via* a non-radical pathway. PMS can work as an inorganic oxidizer to react with SMX through nucleophilic reactions, in

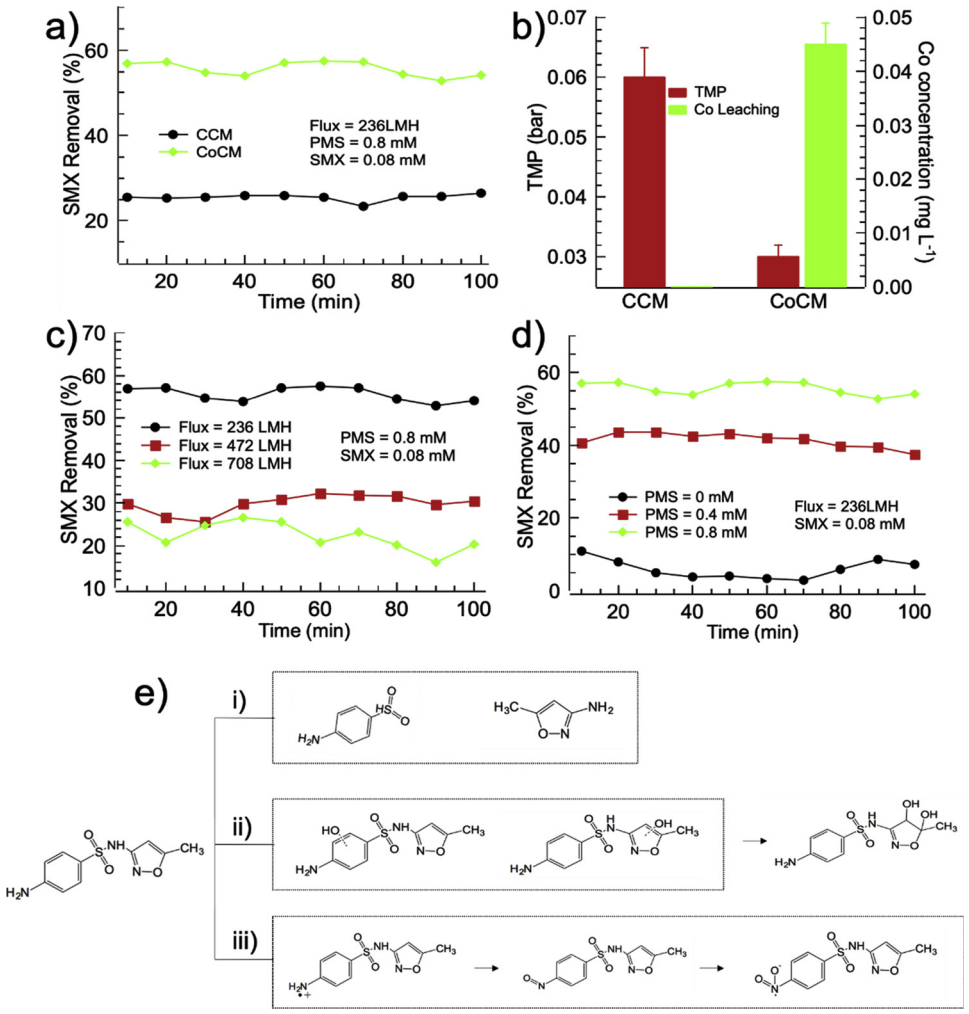

Fig. 4. SMX removal in membrane filtration system (a, effect of membranes; b, records for TMP and Co leaching in 100 min filtration; c, effect of retention time; d, effect of PMS dosage; e, proposed SMX degradation pathway in PMS/CoCM system).

which the S atom of the sulfanilamide group could be selectively attacked. In the radical-pathway, two major radicals ($SO_4^{\bullet -}$ and •OH) were involved in the process, $SO_4^{\bullet -}$ has a highly-selective electrophile mainly acting by electron-transfer from N to $SO_4^{\bullet -}$ yielding to a N-centered radical as a first intermediate (iii), while •OH exhibits high reactivity with olefinic double bonds and anilines [29], therefore, the radical addition on the benzene ring was observed (ii).

3.4. Membrane performance in HA removal

HA is the most ubiquitous natural organic matter (NOM) in the natural aquatic system and it is also present in the effluent of wastewater treatment plant due to its biorecalcitrance. In the membrane filtration system, when the feed was changed to HA solution, the HA removal efficiency increased from 60% (CCM) to ˜100% for CoCM (Fig. 5a). Noticeably, the removal of HA was 46% for CCM at the beginning (< 60 min), and then gradually increased to ˜60% with continuous filtration to 100 min. Meanwhile, the recorded TMP increased from around 0.06 bar to 0.12 bar (Fig. 5b), corresponding to the evolution of membrane fouling by HA cake layer formation, which simultaneously increased the HA removal efficiency. With increasing filtration time the HA molecule would accumulate on the membrane surface, forming a dense cake layer which was related to membrane fouling. The dense cake layer can also function as a rejection layer, through which the HA removal efficiency increased. However, for CoCM, the TMP change was much slower, showing its antifouling property. Meanwhile, the removal of HA was maintained at > 95% throughout the filtration experiment which could be caused by the synergistic effects between membrane separation and catalytic oxidation. Apparently, the generated radicals in CoCM could degrade HA molecules into smaller ones, and thus reduce the membrane pore blocking.

3.5. Membrane performance in SMX-HA removal

In this experiment, the membrane performance was tested when SMX and HA were co-existed in the feed. The SMX removal decreased from ˜60% (10 min) to 46% (100 min) for CoCM (Fig. 6a) while the increase of HA removal after 60 min filtration was observed, indicating the existence of membrane fouling (Fig. 6b). Compared with the single species system (SMX or HA), both SMX and HA removal efficiency decreased in the SMX-HA co-existence system. The decrease in SMX removal is believed to be due to the scavenging of sulfate radical by HA [30], while the decrease in HA removal could be caused by the decrease of active sites on the membrane surface. The results showed that the catalytic performance of CoCM would be partially suppressed in the natural water which consists of recalcitrant bulk organic matters (*e.g.*, humic acid). The AFM images of membranes after filtration test are shown in Fig. 6. The surface roughness was slightly decreased for both CCM and CoCM, which could be caused by the partially deposition of HA on the membrane surface.

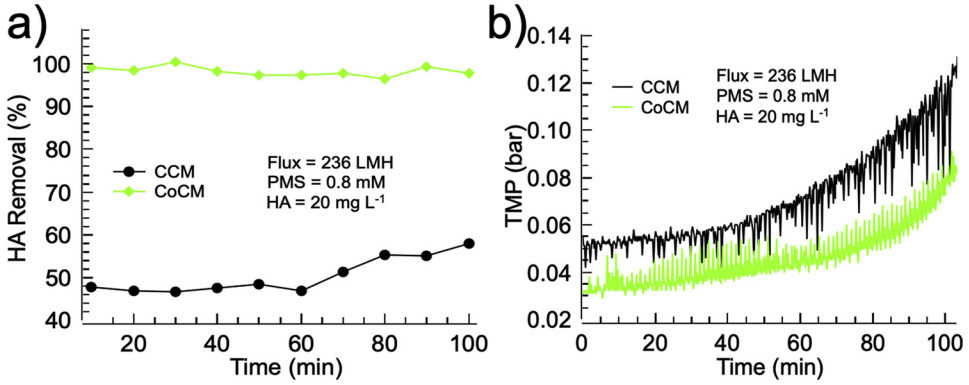

Fig. 5. HA removal (a) and TMP changes (b) in membrane filtration system.

3.6. Membrane fouling elimination in SMX-HA system

Analysis of the time-dependent pressure variations in the membrane filtration system could provide membrane fouling evolution in the process. Three treatment cycles in SMX-HA system over CCM and CoCM were conducted at a constant flux operational mode. For each treatment cycle, the operation time was 100 min followed by the washing with PMS solution for 60 min. As depicted in Fig. 7a, with the prolong of filtration time, TMP increased noticeably for CCM because of the deposition of HA molecules on the membrane surface as well as in the internal pores. As compared with CCM, the TMP increase in CoCM was much slower due to the decomposition of HA *via* radicals. After 100 min filtration, the PMS washing had no significant effect on the flux recovery for both CCM and CoCM, indicating the active sites on CoCM might have been enveloped by HA, resulting in the deactivation of catalyst. To decompose the HA accumulated on the surface of active sites, both CCM and CoCM were regenerated *via* a heat-treatment method at 450 °C for 1 h. Results showed that fully recovery of initial flux could be achieved by this method while the membrane fouling rate increased in the following treatment.

Fig. 7b shows that in the treatment cycles of 1–3, the removal of HA for CoCM slightly increased while the removal of SMX decreased. The increase in HA removal was attributed to the partly membrane fouling, in which rejection of HA by size-exclusion mechanism could take effect. For SMX, once the active sites on catalyst were fouled by HA, the degradation efficiency decreased. For CCM, during three treatment cycles, the HA removal increased while the SMX removal maintained at 15 ± 5% (Fig. 7b). The removal of HA should be mainly caused by the membrane rejection from the cake layer on the surface (Fig. 7c) while the removal of SMX should be caused by the catalytic oxidation by PMS. In comparison with CCM, CoCM did not show the formation of cake layer (Fig. 7c), further confirmed its antifouling property.

3.7. PMS activation and organics removal mechanism in CoCM

In the PMS/CoCM system, $SO_4^{\bullet -}$ and •OH could be formed [31]. Literature reported that methanol can react with •OH and $SO_4^{\bullet -}$ at high and comparable rates with reaction rate constants of $k_{[\bullet OH]} = 1.2–2.8 \times 10^9\ M^{-1}\ s^{-1}$ and $k_{[SO4\bullet-]} = 1.6–7.7 \times 10^7\ M^{-1}\ s^{-1}$ [29,32], while $SO_5^{\bullet -}$ is quite inert toward alcohols because of the low reaction rate which is less than $10^3\ M^{-1}\ s^{-1}$ [32]. Meanwhile, alcohols with no α-hydrogen such as *tert*-butanol (TBA) are more effective in quenching •OH ($3.8–7.6 \times 10^8\ M^{-1}\ s^{-1}$) compared with that of $SO_4^{\bullet -}$ ($4.0–9.1 \times 10^5\ M^{-1}\ s^{-1}$) [33].

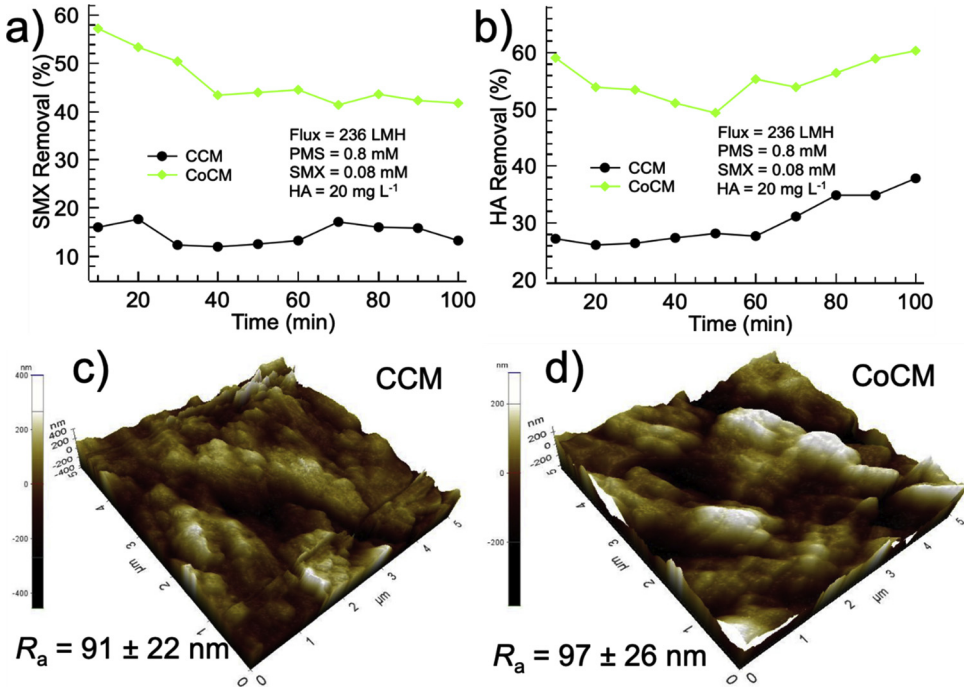

Fig. 6. SMX and HA removal in the SMX-HA system (a and b) and the AFM images of used membranes (c and d).

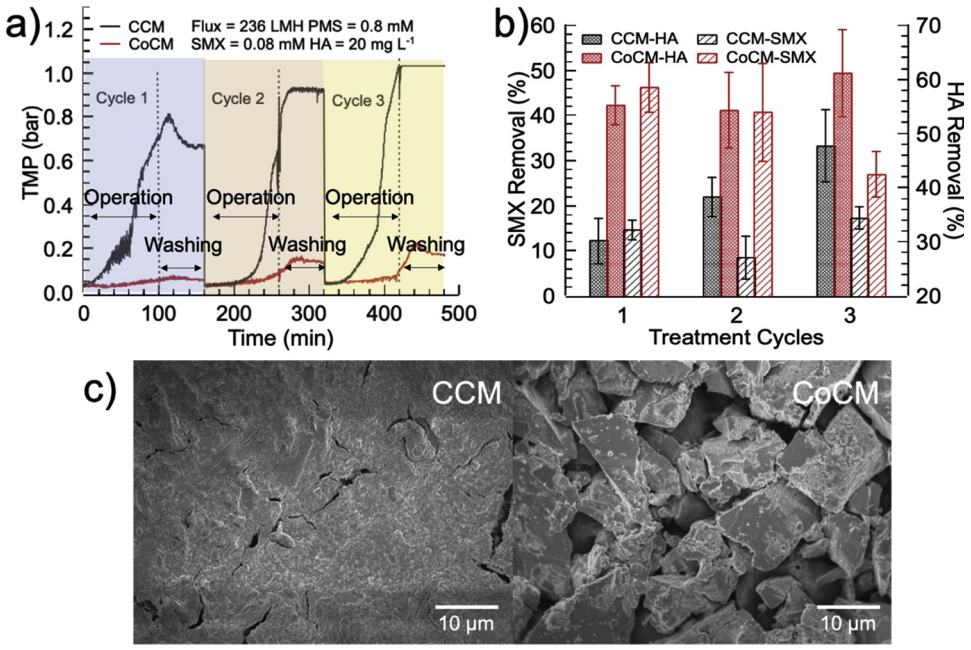

Fig. 7. a) TMP changes and b) SMX and HA removal in different treatment cycles for CCM and CoCM; c) FESEM images of CCM and CoCM after 3 treatment cycles.

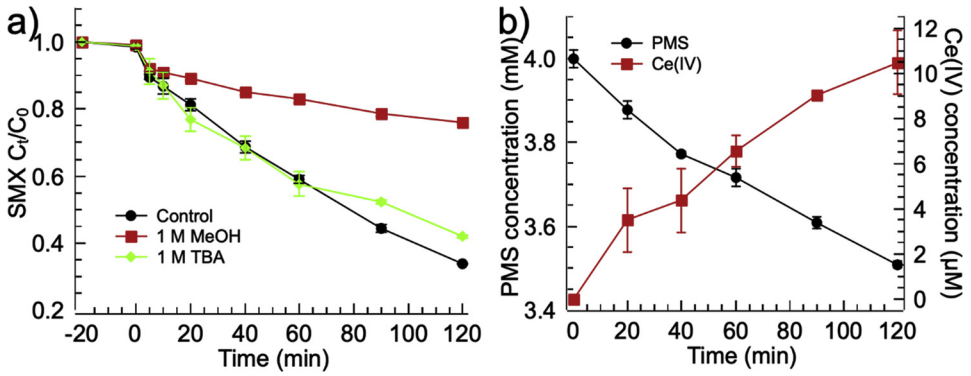

Fig. 8. a) Effect of different scavengers on SMX degradation in PMS/CoCM system (Conditions: [PMS] = 0.4 mM, [SMX] = 0.04 mM); and b) PMS decomposition and the $SO_4^{\bullet -}$ generation in PMS/CoCM system (Conditions: [PMS] = 4 mM, [Ce (III)] = 10 mM).

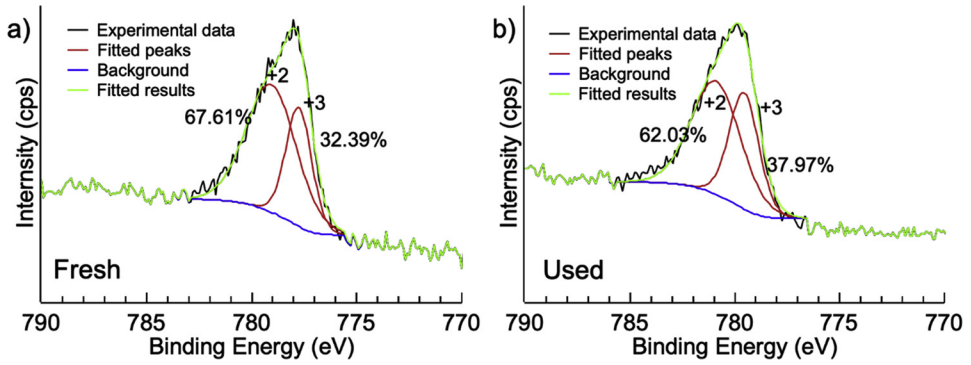

Fig. 9. The high resolution of Co2p in fresh and used CoCM.

To identify the major reactive oxygen species that were responsible for PMS/CoCM system in the degradation of SMX in natural pH, TBA and methanol were used as quenching agents in a batch system [34]. Fig. 8a shows the effect of different scavengers on the degradation of SMX. In the control experiment, the SMX removal could be achieved to 66% in 120 min, while the removal decreased to 24% and 58% when 1 M MeOH and 1 M TBA were added, respectively. The results showed that $SO_4^{\bullet -}$ should be the major contribution in the SMX degradation under the experimental conditions Eqs. (7–9). To further determine the $SO_4^{\bullet -}$ generation process, a PMS self-decomposition experiment without SMX was conducted and the results are shown in Fig. 8b. The calculation of $SO_4^{\bullet -}$ was conducted based on a spectrophotometric method *via* the oxidation of Ce (III) to Ce (IV), which has an adsorption at wavelength of 320 nm [24]. At the initial concentration of 4 mM,

PMS consumption rate was calculated as 12.3% (0.49 mM), while the generated $SO_4^{\bullet -}$ was calculated as 10.5 μM Eq. (6) in 120 min.

$$HSO_5^- + Co^{2+} \rightarrow SO_4^{\bullet -} + Co^{3+} + OH^- \quad (7)$$

$$HSO_5^- + Co^{2+} \rightarrow SO_4^{2-} + Co^{3+} + \bullet OH \quad (8)$$

$$SO_4^{\bullet -} + H_2O \rightarrow SO_4^{2-} + \bullet OH + H^+ \; k[H_2O] < 2 \times 10^{-3}\ s^{-1} \quad (9)$$

$$HSO_5^- + Co^{3+} \rightarrow SO_5^{\bullet -} + Co^{2+} + H^+ \quad (10)$$

Fig. 9 presents the XPS of Co2p of the Co_3O_4 before and after oxidation reaction. The ratio of Co^{2+}/Co^{3+} slightly decreased from 2.09 to 1.63 after reaction, showing Co^{2+} underwent a partial transfer to Co^{3+} in the oxidation process. The ratio of O_A in the O1s spectrum decreased to 76.7% after the reaction (Fig S5), evidencing the electronic transformation process *via* Co^{2+} to Co^{3+}. The oxidizing reaction occurs on the surface and Co^{2+} would provide the electrons Eqs. (7, 8). In order to keep the balance of charge on the catalyst surface, Co^{3+} will accept the electrons from the system Eq. (10). It manifests the involvement of $Co^{2+} - Co^{3+} - Co^{2+}$ redox processes during the reaction. The slight decrease of the ratio of Co^{2+}/Co^{3+} showed that the Co^{3+} could not be fully reduced in the system after a prolonged use of CoCM.

Herein, the radical generation and organics removal in CoCM is proposed as shown in Fig. 10. As analyzed before, Co_3O_4 distributed uniformly on the surface of the Al_2O_3 in the form of Co—O—Al (Fig. 2 SEM analysis and Fig. 3 XPS analysis), forming a conformal coating across both the membrane surface as well as the internal pores. Apparently, the nanocatalytic Co_3O_4 in CoCM functioned as a stable cobalt source to accelerate the generation of radicals from PMS *via* Reactions (7–10). Generally, sulfate radical would be generated by the reduction of HSO_5^- *via* accepting electrons from Co^{2+}, and at the same time, it could be regenerated by reducing from Co^{3+}, in which HSO_5^- was transformed into $SO_5^{\bullet -}$ and H^+ [8]. $SO_4^{\bullet -}$ can further transform into •OH by reacting with H_2O [35]. In the heterogeneous cobalt-catalyzed system, it is believed that the redox cycle of cobalt species occurring in Co_3O_4 facilitates the radical generation. As shown in this work, the leaching of cobalt ions into solutions was minimal since the two different oxides of cobalt were bounded and could interact autogenously [26,36]. For the organics removal in CoCM, part of organics could be rejected by membrane separation *via* size exclusion mechanism. At the same time, radicals produced could degrade the organics into smaller molecular, some of which might pass through the membrane.

3.8. Versatility of in-situ self-scarified template method

One primary benefit of the *in-situ* self-scarified template method reported herein is its versatality for different metal oxides. Theorectically, any metal oxides could be formed *via* this process and disturbuted uniformally across the whole membrane substrate as long as the metal ions can form hydroxide *via* conneting with hydroxyl. Therefore, to investigate the versatality of this method, Mn oxides and Ni oxides impregnated ceramic membranes were prepared *via* the same method, in which cobalt nitrate was replaced by manganese nitrate and nickel nitrate (Figs S6–S8 and Text S1). Results showed that Mn oxides and Ni oxides could be impregnated successfully and uniformly into the membrane pores and both catalytic ceramic membranes showed an enhanced performance in SMX degrdation and HA removal. Thus, the *in-situ* self-scarified template method should be universally applicable for the fabrication of metal oxides impregnated ceramic membranes for water treatment.

4. Conclusions

A novel pore-functionalized ceramic membrane with isotropically impregnated cobalt oxide (CoCM) was prepared *via in-situ* self-scarified template method and used for organics removal in membrane filtration system. Based on the results presented, the following conclusions are drawn:

1) The nanocatalytic Co_3O_4 was distributed evenly and uniformly throughout the whole membrane *via* an *in-situ* self-scarified template method without significantly changing the membrane surface roughness.
2) The CoCM showed high pure water permeability and catalytic performance in SMX-HA system. The SMX removal efficiency could be affected by both contact time and PMS dosage.
3) The formation of Co—O—Al bonding made CoCM more robust and stable with a low cobalt leaching.
4) The CoCM showed an antifouling property and could be regenerated *via* a heat treatment.
5) The Co^{2+}/Co^{3+} ratio change after reaction evidenced the PMS activation and the quantitative calculation of $SO_4^{\bullet -}$ further confirmed the radical generation in the oxidation process.
6) The organics removal in CoCM included catalytic degradation *via* radical generation and membrane separation *via* size-exclusion.

Acknowledgements

The sample characterization (FESEM and XRD) work were performed at the Facility for Analysis, Characterization, Testing and Simulation (FACTS) in Nanyang Technological University, Singapore. The AFM test was conducted in Central Environmental Science and Engineering Laboratory (CESEL), Nanyang Technological University.

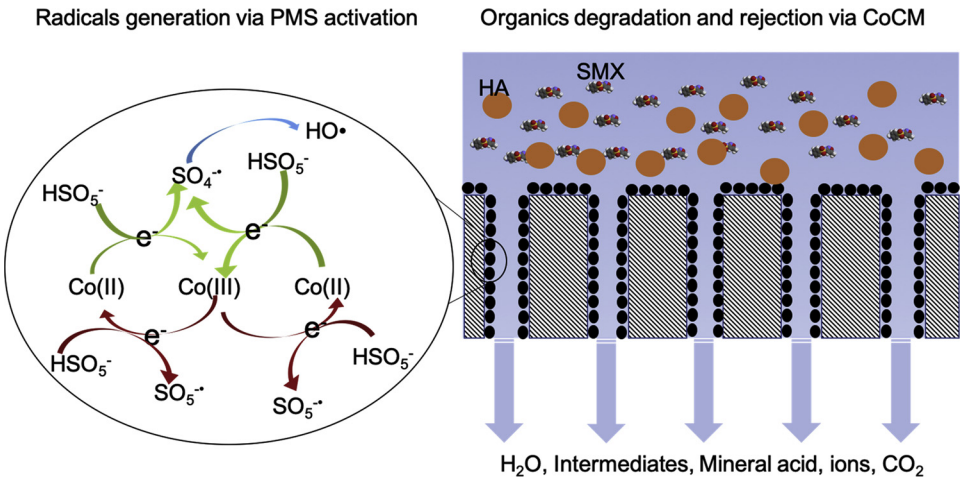

Fig. 10. Schematic illustration of the proposed radical generation and organics removal in CoCM.

Also, the authors would like to thank Nanyang Technological University for the research scholarship.

Appendix A. Supplementary data

Supplementary material related to this article can be found, in the online version, at doi:https://doi.org/10.1016/j.apcatb.2019.04.081.

References

[1] K.D. Brown, J. Kulis, B. Thomson, T.H. Chapman, D.B. Mawhinney, Occurrence of antibiotics in hospital, residential, and dairy effluent, municipal wastewater, and the Rio Grande in New Mexico, Sci. Total Environ. 366 (2006) 772–783.

[2] R. Hirsch, T. Ternes, K. Haberer, K.-L. Kratz, Occurrence of antibiotics in the aquatic environment, Sci. Total Environ. 225 (1999) 109–118.

[3] L. Rizzo, C. Manaia, C. Merlin, T. Schwartz, C. Dagot, M.C. Ploy, I. Michael, D. Fatta-Kassinos, Urban wastewater treatment plants as hotspots for antibiotic resistant bacteria and genes spread into the environment: a review, Sci. Total Environ. 447 (2013) 345–360.

[4] O.M. Rodriguez-Narvaez, J.M. Peralta-Hernandez, A. Goonetilleke, E.R. Bandala, Treatment technologies for emerging contaminants in water: a review, Chem. Eng. J. 323 (2017) 361–380.

[5] W.-D. Oh, Z. Dong, T.-T. Lim, Generation of sulfate radical through heterogeneous catalysis for organic contaminants removal: current development, challenges and prospects, Appl. Catal. B Environ. 194 (2016) 169–201.

[6] H. Li, J. Tian, Z. Zhu, F. Cui, Y.-A. Zhu, X. Duan, S. Wang, Magnetic nitrogen-doped nanocarbons for enhanced metal-free catalytic oxidation: integrated experimental and theoretical investigations for mechanism and application, Chem. Eng. J. 354 (2018) 507–516.

[7] X. Duan, C. Su, J. Miao, Y. Zhong, Z. Shao, S. Wang, H. Sun, Insights into perovskite-catalyzed peroxymonosulfate activation: maneuverable cobalt sites for promoted evolution of sulfate radicals, Appl. Catal. B Environ. 220 (2018) 626–634.

[8] G.P. Anipsitakis, D.D. Dionysiou, Radical generation by the interaction of transition metals with common oxidants, Environ. Sci. Technol. 38 (2004) 3705–3712.

[9] P.R. Shukla, S. Wang, H. Sun, H.M. Ang, M. Tadé, Activated carbon supported cobalt catalysts for advanced oxidation of organic contaminants in aqueous solution, Appl. Catal. B Environ. 100 (2010) 529–534.

[10] W. Chu, W.K. Choy, C.Y. Kwan, Selection of supported cobalt substrates in the presence of oxone for the oxidation of monuron, J. Agric. Food Chem. 55 (2007) 5708–5713.

[11] P. Shukla, S. Wang, K. Singh, H.M. Ang, M.O. Tadé, Cobalt exchanged zeolites for heterogeneous catalytic oxidation of phenol in the presence of peroxymonosulphate, Appl. Catal. B Environ. 99 (2010) 163–169.

[12] T.V. Kon'kova, I.P. Prosvirin, M.B. Alekhina, S.A. Skornikova, Cobalt-containing catalysts based on Al_2O_3 for the oxidative destruction of organic dyes in the aqueous phase, Kinet. Catal. 56 (2015) 206–211.

[13] Y. Zhuang, Q. Lin, L. Zhang, L. Luo, Y. Yao, W. Lu, W. Chen, Mesoporous carbon-supported cobalt catalyst for selective oxidation of toluene and degradation of water contaminants, Particuology 24 (2016) 216–222.

[14] H. Huang, K. Schwab, J.G. Jacangelo, Pretreatment for low pressure membranes in water treatment: a review, Environ. Sci. Technol. 43 (2009) 3011–3019.

[15] N. Lee, G. Amy, J.-P. Croué, H. Buisson, Identification and understanding of fouling in low-pressure membrane (MF/UF) filtration by natural organic matter (NOM), Water Res. 38 (2004) 4511–4523.

[16] C.J. Geankoplis, Transport Processes and Separation Process Principles:(includes Unit Operations), Prentice Hall Professional Technical Reference, 2003.

[17] N. Ma, X. Quan, Y. Zhang, S. Chen, H. Zhao, Integration of separation and photocatalysis using an inorganic membrane modified with Si-doped TiO_2 for water purification, J. Membr. Sci. 335 (2009) 58–67.

[18] R. Goei, T.-T. Lim, Ag-decorated TiO_2 photocatalytic membrane with hierarchical architecture: photocatalytic and anti-bacterial activities, Water Res. 59 (2014) 207–218.

[19] Y. Zhang, C. He, V.K. Sharma, X. Li, S. Tian, Y. Xiong, A coupling process of membrane separation and heterogeneous Fenton-like catalytic oxidation for treatment of acid orange II-containing wastewater, Sep. Purif. Technol. 80 (2011) 45–51.

[20] L.M. Corneal, M.J. Baumann, S.J. Masten, S.H. Davies, V.V. Tarabara, S. Byun, Mn oxide coated catalytic membranes for hybrid ozonation-membrane filtration: membrane microstructural characterization, J. Membr. Sci. 369 (2011) 182–187.

[21] B.S. Karnik, S.H. Davies, M.J. Baumann, S.J. Masten, Fabrication of catalytic membranes for the treatment of drinking water using combined ozonation and ultrafiltration, Environ. Sci. Technol. 39 (2005) 7656–7661.

[22] Y. Bao, W.-D. Oh, T.-T. Lim, R. Wang, R.D. Webster, X. Hu, Surface-nucleated heterogeneous growth of zeolitic imidazolate framework–a unique precursor towards catalytic ceramic membranes: synthesis, characterization and organics degradation, Chem. Eng. J. 353 (2018) 69–79.

[23] J.T. Richardson, Principles of Catalyst Development, Springer, 2013.

[24] W. Chen, R. Chen, R. Zhang, N. Zhang, imple spectrophotometric determination of sulfate free radicals, Anal. Methods 10 (2018) (2018) 3470–3474.

[25] M.C. Biesinger, B.P. Payne, A.P. Grosvenor, L.W. Lau, A.R. Gerson, R.S.C. Smart, Resolving surface chemical states in XPS analysis of first row transition metals, oxides and hydroxides: Cr, Mn, Fe, Co and Ni, Appl. Surf. Sci. 257 (2011) 2717–2730.

[26] G.P. Anipsitakis, E. Stathatos, D.D. Dionysiou, Heterogeneous activation of oxone using Co_3O_4, J. Phys. Chem. B 109 (2005) 13052–13055.

[27] F. Chen, X. Shi, X. Chen, W. Chen, An iron (II) phthalocyanine/poly (vinylidene fluoride) composite membrane with antifouling property and catalytic self-cleaning function for high-efficiency oil/water separation, J. Membr. Sci. 552 (2018) 295–304.

[28] Y. Bao, W.-D. Oh, T.-T. Lim, R. Wang, R.D. Webster, X. Hu, Elucidation of stoichiometric efficiency, radical generation and transformation pathway during catalytic oxidation of sulfamethoxazole via peroxymonosulfate activation, Water Res. 151 (2019) 64–74.

[29] G.V. Buxton, C.L. Greenstock, W.P. Helman, A.B. Ross, Critical review of rate constants for reactions of hydrated electrons, hydrogen atoms and hydroxyl radicals ($\cdot OH/\cdot O^-$ in aqueous solution, J. Phys. Chem. Ref. Data 17 (1988) 513–886.

[30] Y. Bao, T.-T. Lim, R. Wang, R.D. Webster, X. Hu, Urea-assisted one-step synthesis of cobalt ferrite impregnated ceramic membrane for sulfamethoxazole degradation via peroxymonosulfate activation, Chem. Eng. J. 343 (2018) 737–747.

[31] G.P. Anipsitakis, D.D. Dionysiou, Degradation of organic contaminants in water with sulfate radicals generated by the conjunction of peroxymonosulfate with cobalt, Environ. Sci. Technol. 37 (2003) 4790–4797.

[32] E. Hayon, A. Treinin, J. Wilf, Electronic spectra, photochemistry, and autoxidation mechanism of the sulfite-bisulfite-pyrosulfite systems. SO_2^-, SO_3^-, SO_4^-, and SO_5^- radicals, J. Am. Chem. Soc. 94 (1972) 47–57.

[33] Y. Feng, D. Wu, Y. Deng, T. Zhang, K. Shih, Sulfate radical-mediated degradation of sulfadiazine by $CuFeO_2$ rhombohedral crystal-catalyzed peroxymonosulfate: synergistic effects and mechanisms, Environ. Sci. Technol. 50 (2016) 3119–3127.

[34] L. Xu, J. Wang, A heterogeneous Fenton-like system with nanoparticulate zero-valent iron for removal of 4-chloro-3-methyl phenol, J. Hazard. Mater. 186 (2011) 256–264.

[35] P. Hu, M. Long, Cobalt-catalyzed sulfate radical-based advanced oxidation: a review on heterogeneous catalysts and applications, Appl. Catal. B Environ. 181 (2016) 103–117.

[36] W. Zhang, H.L. Tay, S.S. Lim, Y. Wang, Z. Zhong, R. Xu, Supported cobalt oxide on MgO: highly efficient catalysts for degradation of organic dyes in dilute solutions, Appl. Catal. B Environ. 95 (2010) 93–99.